Influence of Cr on the Surface Properties of the Micro-Textured WC+Co Alloy Coating

Xin Tong, Qiang Qu *, Yu Zhang and Pei Han

Key Laboratory of Advanced Manufacturing and Intelligent Technology, Harbin University of Science and Technology, Harbin 150080, China
* Correspondence: quqiang0929@163.com

Abstract: In this paper, we investigated the effect of Cr on the surface properties of the micro-textured WC+Co alloy coating. An interactive test was designed that considered the parameters of an AlSiTiN coating and an AlSiTiN–AlCrN double coating. Using hardness and phase composition as evaluation criteria, the influence of Cr on the mechanical properties and microstructure of the coating surface was analyzed. A friction and wear test platform was formed to explore the mechanism of the Cr influence on the friction performance and wear state of the coating surface. The results show that Cr leads to the generation of the α-Cr phase particles in the surface structure of the specimen. They easily combine with C to form carbides, which improve the coating hardness; the atomic radius of Cr is smaller than that of Al, so it can dissolve in AlN. This induces lattice distortion, changing the phase composition in the structure; the coating with Cr exhibits better surface friction performance and wear morphology, simultaneously generating enhanced mechanical vibrations.

Keywords: elementary Cr; coating; hardness; phase; surface properties; friction

1. Introduction

Cemented carbides have been widely used in the machining field due to their high hardness and strength [1]. Among them, WC+Co alloy is a typical tool material with high bending strength and good thermal conductivity but poor heat and wear resistance. It was shown that machining a suitable micro-texture on the surface of cemented carbides can reduce the cutting force and cutter wear and prolong the cutter's service life, leading to better machining quality of the workpiece surface [2]. Coating the alloy surface by vapor deposition can also improve the heat resistance and wear resistance of cemented carbide. AlSiTiN and Cr have been widely used coatings because of their stable chemical properties, good thermal stability and oxidation resistance.

Many research studies have been conducted on micro-texturing and coating of cemented carbides. Wang et al. [3] performed laser micro-texturing on the friction pair surface. Under oil lubrication conditions, they used a universal friction and wear testing machine to conduct friction and wear experiments, examining the worn surface using three-dimensional ultra-depth-of-field microscopy. The results showed that the micro-texture effectively stored wear abrasive particles to reduce the friction surface damage caused by secondary wear. Guimaraes B. et al. [4] proposed a laser surface texture method for WC–Co green pressed billet to obtain different micropatterns for drawing cross shadow lines to enhance the wettability of these tools. The results show that the laser surface texturization can produce well-defined, reproducible and equispaced micropatterns for drawing cross shadow lines in WC–Co green compact. Zhang Jin et al. [5] prepared Sn-Ag-Cu (SAC)-filled micro-textured composite anti-wear surfaces (CASs). The tribological and frictional noise characteristics of CASs and smooth surfaces (SS) with different texture spacings during dry sliding friction were experimentally investigated and analyzed in detail. The CAS significantly improved the tribological properties and noise suppression

performance. Xu et al. [6] studied the effect of pulsed laser parameters on the morphology and area occupancy of micro-textured micro-pits on the surface of a cylinder liner and its further influence on the friction and wear properties of friction pairs and determined the underpinning action mechanism. It was found that the micro-texture improved the friction of cylinder liner friction pairs. The mechanism of improved wear performance assumes storing lubricating oil, reducing the contact area of the friction pair, capturing wear debris and decreasing abrasive wear. Zhang et al. [7] designed micro-texture with good lubricating properties using simulations, then optimized the laser processing parameters to match the simulation results and the micro-texture on the surface of the upper guide rail, and studied the effect of the micro-texture using friction and wear tests. The existence of the micro-texture generated hydrodynamic pressure and increased the load. Yan et al. [8] summarized the research progress of coating tribology, reviewed the research status of the friction and wear characteristics of common coatings, and analyzed the wear and damage mechanisms of various coatings in the friction process. It was found that the wear resistance of coated workpieces is mainly related to the coating properties in the contact zone. Once the coating is worn off, the substrate takes the wear resistance role. Dong et al. [9] used fiber coaxial laser cladding equipment to clad Fe-Cr-Mo-Si alloy powder on the surface of Q235 steel and prepared a wear-resistant cladding layer based on the iron alloy. A Vickers hardness tester and a friction and wear testing machine were used to study the microstructure, hardness and friction and wear behavior of the Fe-Cr-Mo-Si cladding layer. The results show that the laser cladding Fe-Cr-Mo-Si alloy powder on the surface of Q235 steel significantly improved the wear resistance of the material. Zhang Yiyong et al. [10] prepared FeCrAl alloy with low Cr content and studied the crystal structure, microstructure, tensile properties and high-temperature steam oxidation resistance of FeCrAl alloy with low Cr content. With the decrease in Cr content, the matrix phase of Fe-Cr Al alloy is still in the α-ferritic phase, but the lattice parameters of the matrix phase increase gradually. Reducing Cr content makes the oxidation resistance of Cr-depleted alloy worse, which is still better than that of traditional Zr alloy. Amanov et al. [11] used ultrasonic nanocrystals to modify the surface of Cr_2O_3 and Cr_3C_2-NiCr coatings. The X-ray diffraction patterns and transmission electron microscopy images of the coatings after the UNSM treatment showed small grains of the coatings, which improved the coating hardness. The results of the fuel-lubricated tribology test showed that UNSM reduced the friction coefficient and the specific wear rate of the coating.

However, these studies are limited to considering the separate effects of micro-texture and coating, and they did not address either the synergistic effect of these two factors or provide in-depth research on the effect of Cr on the coating. In this paper, we designed the interaction experiment between micro-texturing and coating parameters based on the surface micro-texture and coating technology. We constructed an experimental platform to study hardness and phase composition, while friction and wear tests were performed to assess the influence mechanism of micro-texturing and coating parameters on the coating hardness. The working mechanism of the micro-textured coating was explored, and the mechanism of the Cr coating's influence on the surface mechanical properties and friction properties of the composite coating was analyzed.

2. Effect of Cr Coating on Surface Hardness and Phase of WC+Co Alloy Composite Coating

2.1. Test Conditions

The AlSiTiN coating experiment was designed as a six-factor, three-level interactive experiment, which considered the following six factors: coating thickness, laser power, scanning speed, scanning times, micro-texture diameter and micro-texture spacing. The specific experimental parameters are listed in Table 1.

Table 1. Six-factor, three-level interactive experiments.

Factor Level	Coating Thickness *h* (mm)	Laser Power *p* (W)	Scan Speed *v* (mm/s)	Scans Times *n* (times)	Micro-Texture Diameter *d* (μm)	Micro-Texture Spacing *l* (μm)	*h* × *d*	*p* × *d*	*v* × *d*	*n* × *d*
1	2.6–2.7	35	1500	6	40	130	1	1	1	1
2	2.8–2.9	40	1600	7	50	150	2	2	2	2
3	3.0–3.1	45	1700	8	60	170	3	3	3	3

When the number of coating layers is two, the influence of the coating thickness is not considered, as the detection of the thickness of the double coating is limited, and the total coating thickness of the two layers is determined to be consistent. Based on this, the AlSiTiN–AlCrN double-coating interactive experiment was designed using five-factor and three-level orthogonal experiments. The specific experimental parameters are listed in Table 2.

Table 2. Five-factor and three-level orthogonal experiments.

| Factor Level	Laser Power *p* (W)	Scan Speed *v* (mm/s)	Scans Times *n* (times)	Micro-Texture Diameter *d* (μm)	Micro-Texture Spacing *l* (μm)	*h* × *d*	*p* × *d*	*v* × *d*	*n* × *d*
1	35	1500	6	40	130	1	1	1	1
2	40	1600	7	50	150	2	2	2	2
3	45	1700	8	60	170	3	3	3	3

The experimental coating was prepared by cathode arc ion plating in physical vapor deposition. The specific parameters are as follows: the pressure range is $p < 0.8$ Pa, the furnace chamber is heated to 450 °C, the heating time is 1.5 h, then Ar gas is injected into the furnace chamber, the plasma etching cleaning time is 40 min. Then, the argon was shut off and then the reaction gas nitrogen was passed through. Finally, the workpiece was cooled to 180 °C under vacuum for 2 h [12], and fiber lasers were used to prepare micro-textures. The specific process flow is shown in Figure 1. The selected processing parameters are as follows: a laser wavelength of 1064 nm and a maximum laser output power of 45 W. A scanning electron microscope (SEM) with an X-ray energy dispersive analyzer (EDS) was used to examine the three-dimensional morphology and analyze the surface elemental composition. The hardness was measured by a hardness tester. The method of hardness measurement is to place the specimen in the tray of the hardness tester, and apply different loads to the specimen, and stop applying the load after the hardness value is stable. (The hardness testing instrument used in the experiment is HR-150DT electric Rockwell hardness tester from Harbin, China, for metal steel; the phase detection instrument used in the experiment is JV-DX X-ray diffractometer from Berlin, Germany; the scanning electron microscope used in the experiment is the Zeiss EVO10 high resolution electron microscope from Berlin, Germany).

In the process of laser processing micro-texture, the laser power will increase with the number of micro-textures in a single processing. Therefore, it is difficult to ensure that the depth of micro-texture reaches the ideal value, and existing studies have shown that micro-pits depth has little effect on cutting performance, so this paper does not take micro texture depth as the research content.

2.2. Effect of the Cr Coating on Surface Hardnesst

The hardness test and range analysis results of the AlSiTiN and AlSiTiN–AlCrN coatings are shown in Figure 2a. For the AlSiTiN coating, the coating thickness shows the greatest influence on surface hardness, whereas the laser scanning speed and the micro-texture spacing exhibit a synergistic effect. The second effect is that the number of scans exhibits the least impact among the investigated parameters. The coating thickness shows the greatest influence due to higher amounts of Si and Al in the coating with a higher thickness. Si is a constituting element of diamond and exhibits a diamond crystal

structure; the content of Al affects the coating thickness. Therefore, the bonding strength inside the layer changes under the action of Si and Al, and as a result, the change in the coating thickness greatly influences the hardness value. Compared with other factors, the synergistic effect of the laser scanning speed and micro-texture spacing are also relatively large because, as the scanning speed increases, the time of the material in the laser spot area shortens, and the amount of removed material decreases. Thus, the surface of the workpiece retains a higher fraction of the original WC+Co composition before coating. The increase in the micro-texture spacing enlarges the coating area outside micro-pits during coating compared with the surface with a small micro-texture spacing, yielding a higher hardness. The number of scans exhibits the minuscule effect because the experimental process sequence assumes preparing the micro-texture first and then inserting the coating. The number of scans affects only the depth of micro-pits. Thus, the thickness of the coating in the micro-pits is not affected, so the number of scans exhibits a minimal effect on the coating hardness. Figure 3 shows the enlarged SEM images of the two coatings.
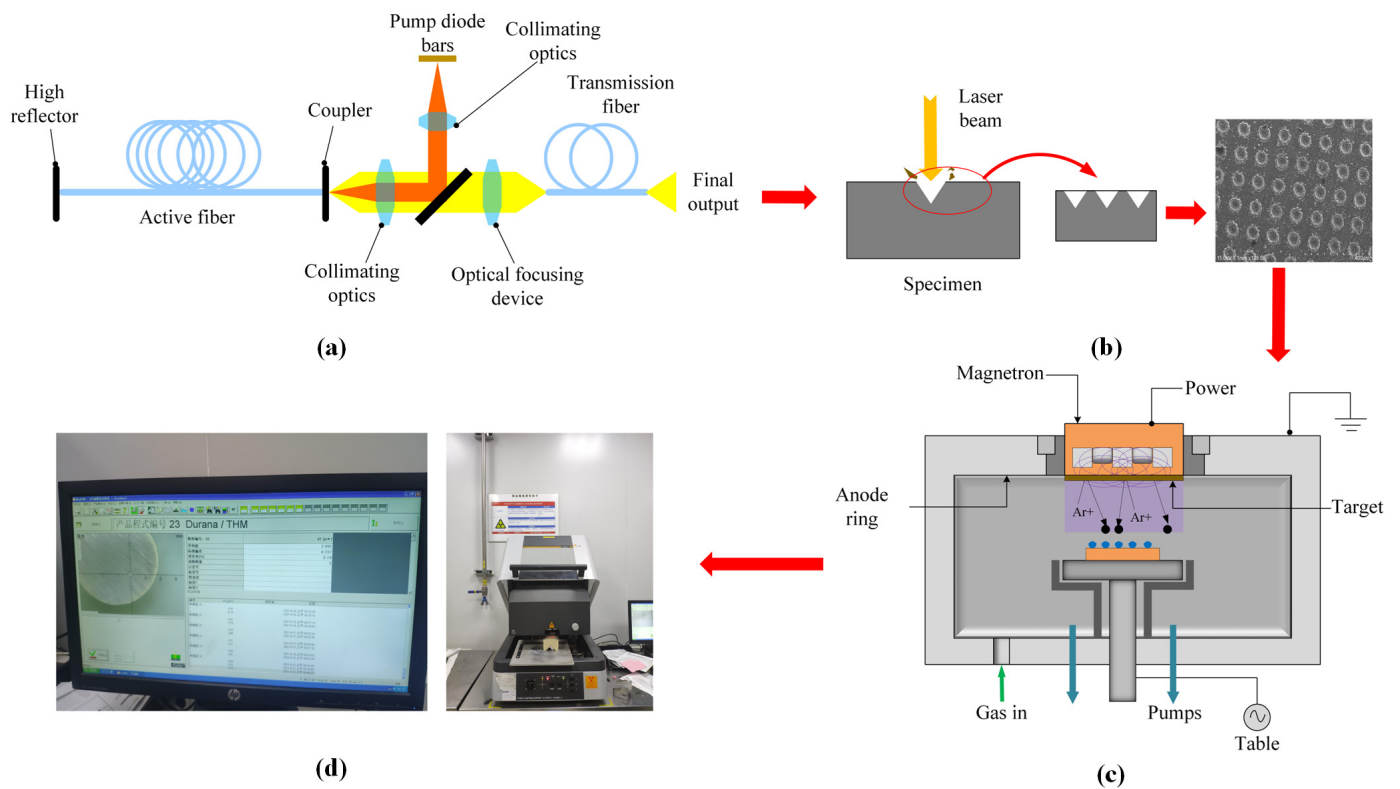

Figure 1. Process flow. (**a**) Principle of Fiber Laser, (**b**) Microtexture preparation, (**c**) Coating Thickness Measuring Instrument, (**d**) Principle of Vapor Deposition.

The hardness value data in Figure 2c indicate that the surface hardness of the AlSiTiN–AlCrN coating specimen is higher than that of the AlSiTiN coating specimen. The variation of surface hardness with the Cr content of the AlSiTiN–AlCrN coating specimen is shown in Figure 2b. The surface hardness value of the test piece is positively correlated with the Cr content; the higher the Cr content, the greater the surface hardness of the test piece. By observing Figure 3, we can see the reason for this. This is because the addition of Cr leads to the formation of the α-Cr phase particles in the surface structure of the specimen (the black part in the figure is the α-Cr particles that can be observed after treatment). These particles exhibit a metallographic structure, significantly improving the structural hardness and providing better structural stability [13]. With the continuous increase in the Cr content, the amount of the precipitated phase α-Cr gradually increases, and the distribution is relatively uniform. Its shape changes from the spherical and short-rod shape to the large-size blocky and flaky shape, greatly improving the microstructural hardness.

This is also related to the formation of carbides. The increase in the Cr content leads to an increase in the carbide content in the material, and hard carbide particles improve the matrix hardness [14]. The hardness value distribution of the AlSiTiN–AlCrN coating specimen is very uniform because the defects, such as voids and pores, in the composite coating layer, diminish with the Cr content, and the quality of the microstructure improves. The precipitated α-Cr phase gradually changes from fine spherical particles to large blocks. They are evenly distributed around the Al and Ti phases, so the strengthening effect of the second phase becomes more pronounced. At the same time, the intergranular AlN/TiN eutectic structure and bulk α-Cr are interconnected to form a uniformly distributed network structure, which is also conducive to promoting the stabilization of microhardness.
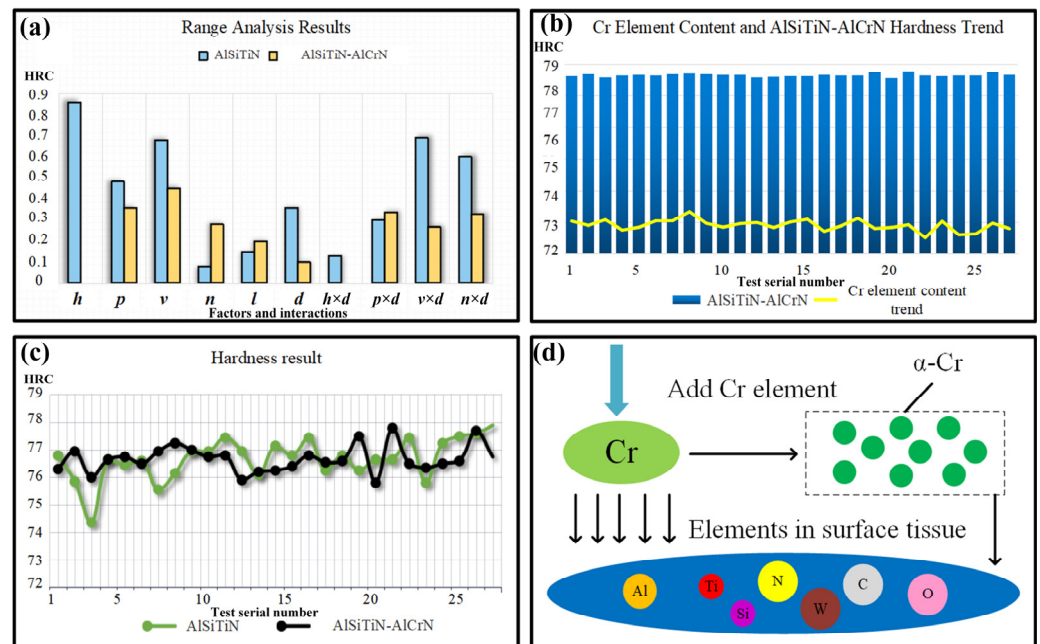
Figure 2. Hardness test results and the action mechanism. (**a**) hardness test range analysis results, (**b**) Cr element content and AlSiTiN–AlCrN hardness trend, (**c**) hardness test results, (**d**) the schematic diagram of Cr element addition.
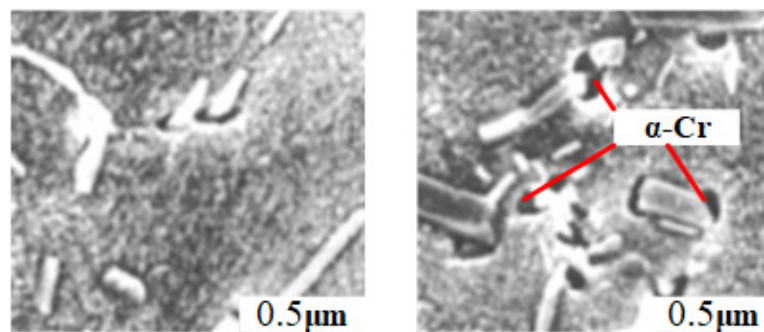

Figure 3. Metallographic diagram (**a**) with or (**b**) without Cr coating.

2.3. Influence of the Cr Coating on the Surface Phase Composition

The elemental composition of the material surface was analyzed using X-ray energy dispersive analysis (EDS), as shown in Figure 4. The upper part represents the EDS spectrum of the AlSiTiN–AlCrN coating, and the lower part is the line-scanning analysis of the elemental content. The Al content inside the micro-pits is much lower than outside

because Al easily reacts with O to form a thin film of chemically stable Al_2O_3 on the surface. The content of other elements inside and outside the micro-pits does not show a significant difference. The content of C is positively correlated with the Cr content, i.e., areas with a high Cr content also exhibit more C than other areas. Since Cr is a strong carbide-forming element, it strongly reacts with carbon and can form special carbides under appropriate conditions if there is enough carbon. In the absence of carbon, it dissolves into a solid atomic solution, and Cr inhibits carbon graphitization.

(a)

(b)

(c)
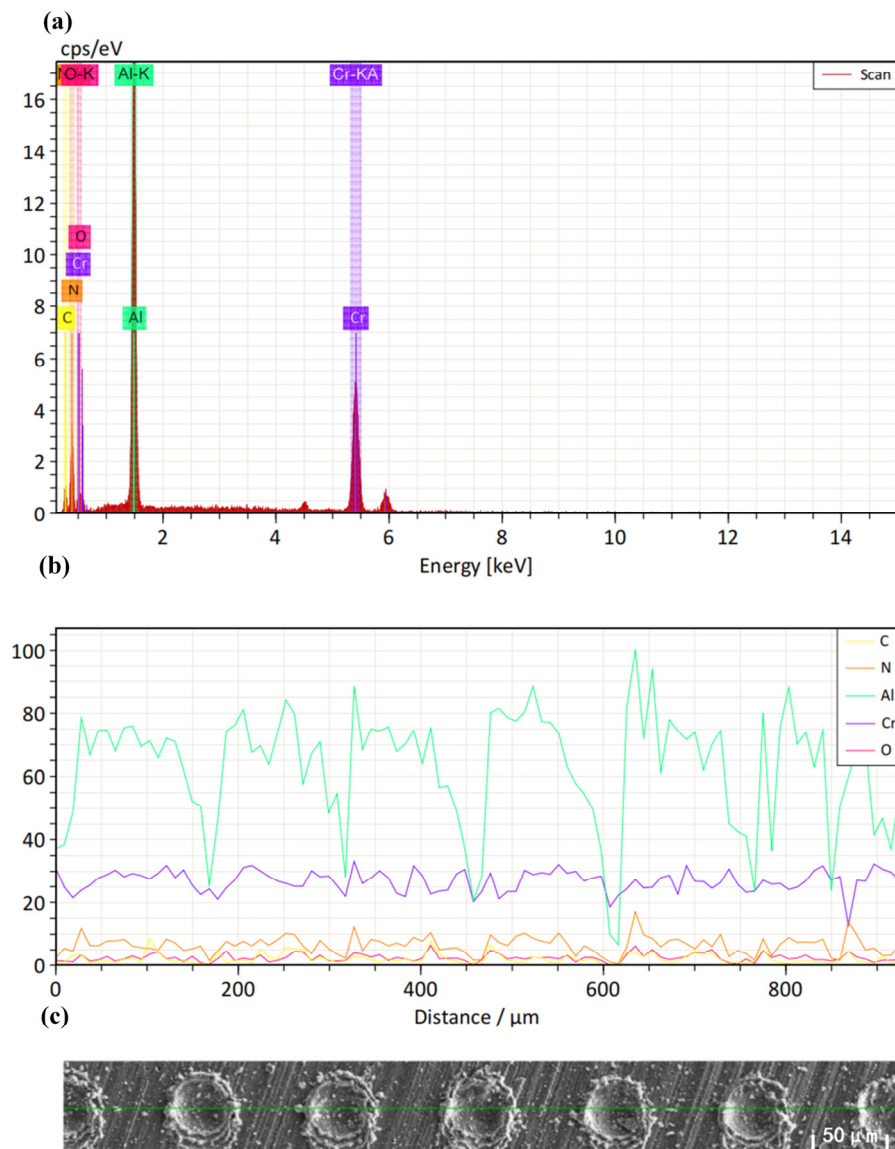
Figure 4. EDS line-scanning elemental analysis of the AlSiTiN–AlCrN coating. (**a**) XRD energy spectrum. (**b**) Line scan element content diagram. (**c**) Line scan local map.

The experimental results of the groups of the two coatings were selected for the XRD phase analysis, and the obtained XRD patterns are shown in Figures 5 and 6. The main peak of the AlSiTiN coating is the WC peak because W is a stronger carbide-forming element than Cr, and it readily forms a compound when the C content is small, so W and C are the main constituting elements of the matrix. By comparison, the addition of Cr causes the replacement of Al and Ti nitrides by CrN. The α-Cr phase in the microstructure gradually changes from the granular to lamellar structure with the Cr content, which is related to the Al and Ti nitride eutectic structures in the layer, reducing the contents of Al and Ti [14]. The number of electrons in the outermost shell of Cr is 1, whereas the number of electrons

in the outermost shell of Al and Ti is 2. Cr and Ti belong to the same period, and the number of electrons of Cr is greater than of Ti, so the electrons of Cr more easily combine with non-metallic elements to form final compounds. When Al, Ti and Cr coexist in the structure, C and N preferentially react with Cr electrons, hindering Al and Ti's interaction with non-metals to form final compounds, as shown in Figure 7.
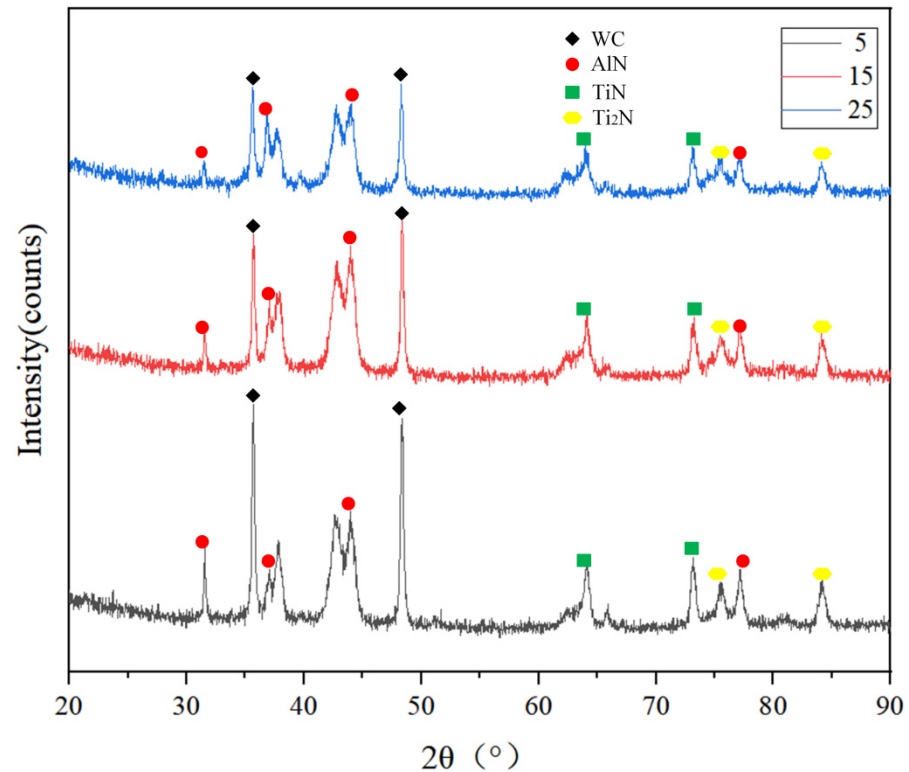
Figure 5. X-ray diffraction pattern of the AlSiTiN coating.

The XRD energy spectrum was analyzed by Jade 5.0 software, and the peak height, peak half width, X-ray wavelength and diffraction angle of each diffraction peak were obtained. And according to the Equation (1) [15]:

$$D = \frac{k\lambda}{\beta cos\theta} \tag{1}$$

where k is a constant; λ is X-ray wavelength, (nm); β is the half width and height of the diffraction peak, (nm); θ is the diffraction angle, (°); D is grain size, (nm).

The value of k is related to the definition of β, usually 0.89. The constant k, X-ray wavelength λ and diffraction angle θ are fixed values. When the half width and height β increase, the grain size D decreases. It can be seen from Figure 8 that the addition of Cr element increases the full width at half maximum of AlN and WC peaks, so the grain size of AlN and WC decreases and the crystal strength increases.
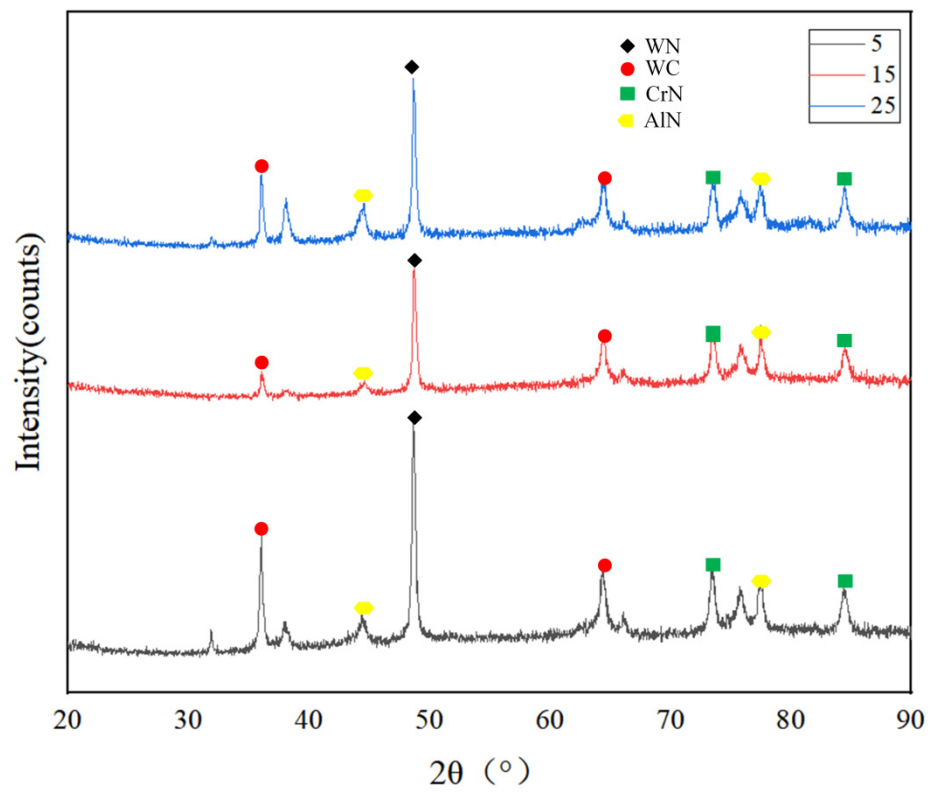
Figure 6. X-ray diffraction patterns of the 5th, 15th and 25th groups of AlSiTiN–AlCrN coatings.
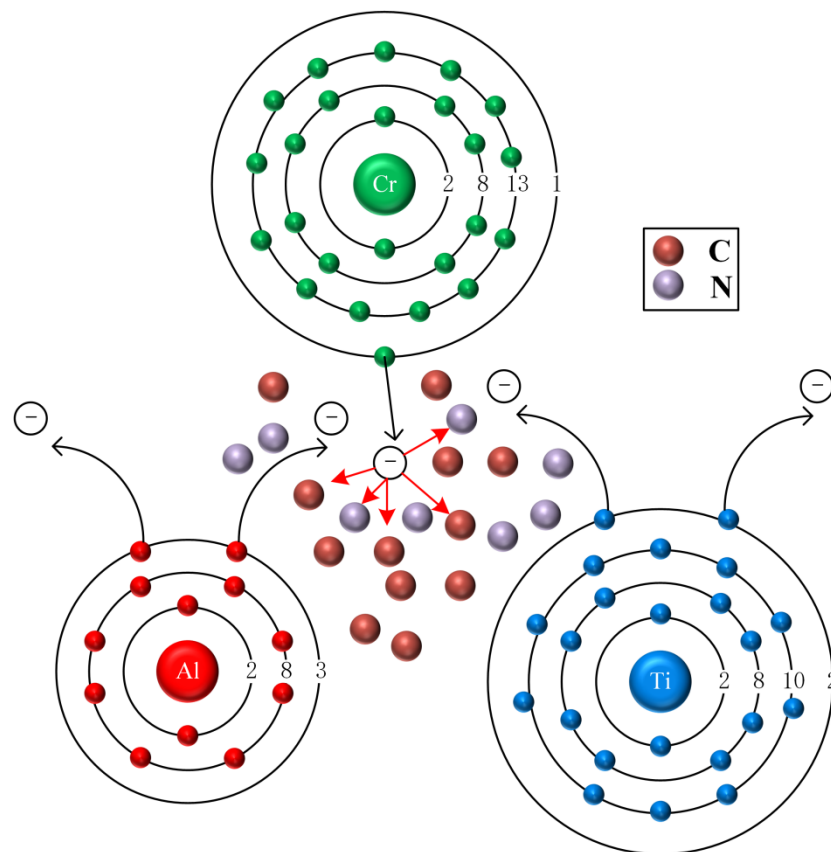

Figure 7. Schematic diagram of gain and loss of electrons of Al, Ti and Cr in the coating structure.

Since the atomic radius of Cr is larger than that of Al, the sign of the misfit degree of Al and Cr in the matrix is opposite. Al reduces the distortion energy in the matrix so that the tendency of these atoms to segregate at grain boundaries and other regions is reduced. Al has slightly lower segregation energy than Cr, indicating that Al occupies the grain boundary positions more preferentially than Cr. When it increases, the segregation energy of Cr becomes negative, and Cr preferentially occupies the grain boundary positions. Regardless of the chemical or mechanical effect, Al weakens grain boundaries and behaves as a brittle impurity, whereas Cr exhibits different behavior. Cr exerts a stronger chemical effect on grain boundary strengthening, whereas its mechanical effect weakens grain boundary bonding. Altogether, Cr can enhance grain boundary bonding and behaves as a tough impurity. When the content of Cr increases, its ability to enhance the bonding of grain boundaries is more prominent. The effect of Al weakening of grain boundaries is offset, and the grains in the microstructure combine at the grain boundaries under the action of Cr, thus realizing the overall grain boundary. In refinement, the peak intensity of each phase successively decreases, as shown in Figure 9. This phenomenon indicates that Cr can keep Al away from the grain boundaries, reduce the peak height of the AlN phase and the grain size of the Al compound and realize grain refinement. The toughness of the composite coating is enhanced, the brittleness is reduced, and the surface properties of the alloy coating are improved. This is consistent with the conclusion that the Cr element in the steel increases and the strength increases in the literature [16].
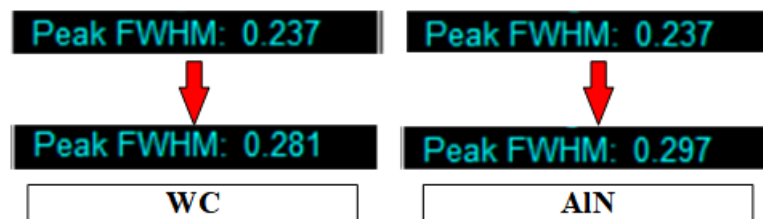

Figure 8. The half width and height of WC and AlN peaks change after adding Cr element.
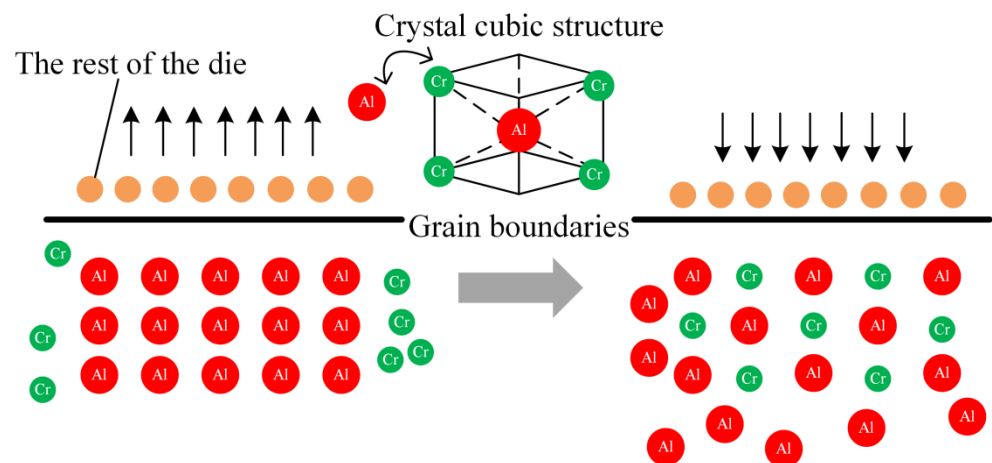

Figure 9. Effects of Cr and Al at grain boundaries.

3. Effect of the Cr Coating on the Friction Properties of Micro-Textured WC+Co Alloy Surfaces

3.1. Construction of the Friction and Wear Experimental Platform

Friction and wear experiments were carried out using a friction and wear machine to measure friction force and friction coefficient. The test environment was a dry environment at room temperature. The selected device for the test was a CETR multi-functional friction and wear tester produced in San Francisco, CA, USA, and the vibration test instrument was a Chengke CT1010SLFP triaxial acceleration sensor produced in Dallas, TX, USA. The test

process parameters were as follows: an applied load of 40 N, a friction distance of 18 mm, a rotation speed of 100 m/min and a friction time of 30 min. The rotating disc in the friction and wear machine consisted of a disc and a pin. The pin was a metal cylinder with a height of 15 mm, a diameter of 6 mm and a chamfer of 0.5 mm. The diameter of the rotating disk was 50.8 mm, the thickness was 6.35 mm, the center hole of the rotating disk was a #10–32 threaded hole through-hole, the center distance between the center hole and the pin was 11.18 mm and the surface roughness was 0.05 μm.

3.2. Influence of the Cr Coating on Surface Vibration Characteristics

In the friction and wear experiment, the vibration acceleration of the surface of the WC+Co cemented carbide pin was recorded by measurements at different periods, and each sample was analyzed at seven time points. The vibration acceleration of the AlSiTiN coating and the AlSiTiN–AlCrN coating in the three X, Y and Z directions in the current period was measured with an acceleration sensor. The obtained sample acceleration data at seven time points are averaged, and the results are shown in Figure 10.
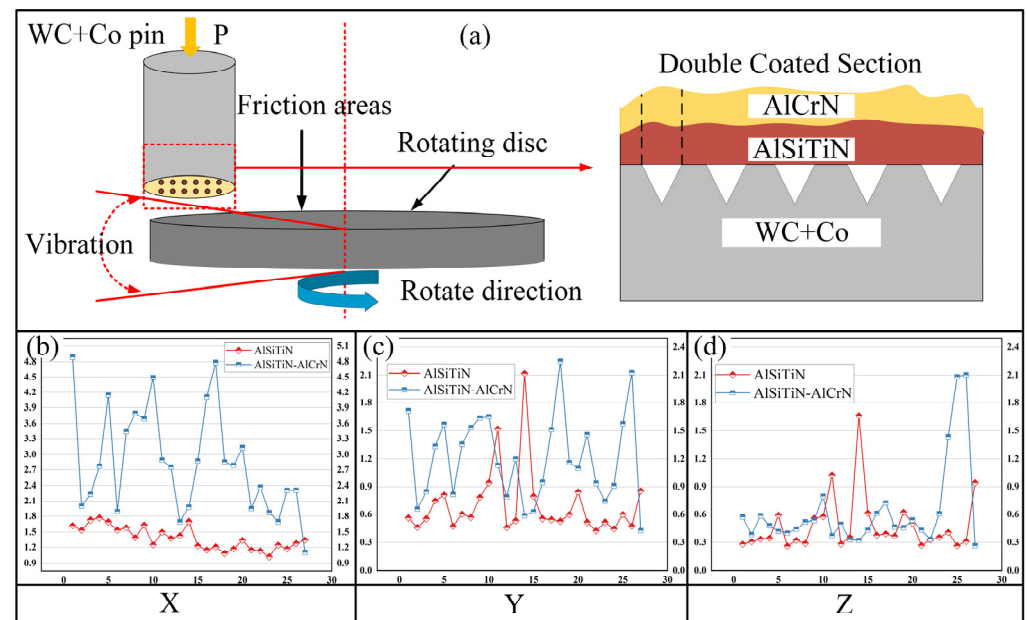
Figure 10. Vibration test results. (**a**) Vibration experiment operation diagram. (**b**) Vibration experimental data in X direction. (**c**) Vibration experimental data in Y direction. (**d**) Vibration experimental data in Z direction.

The data in Figure 10 indicate that the vibration acceleration of the AlSiTiN–AlCrN coating containing Cr in the three X, Y and Z directions is higher than that of the AlSiTiN coating, which is the most pronounced in the X- direction. It shows that coating differences lead to different vibration sizes. The addition of Cr induces greater mechanical vibrations of the coating during the friction and wear experiments.

The reason for this result is that the addition of Cr enriches the AlSiTiN–AlCrN coating with more α-Cr phase particles in the surface structure compared to than the AlSiTiN coating, easily combining with C in the alloy to form Cr-containing particles, which greatly improves the surface hardness of the AlSiTiN–AlCrN coating. The hardness of the workpiece material exhibits a significant effect on the vibration acceleration difference between the workpiece and the rotating disk in all directions mainly because the temperature of the area where the workpiece coating surface and the surface of the grinding disk are in contact rises rapidly when the rotation value of the workpiece containing a high hardness material exceeds a certain value, so the softening effect of the material occurs. The coating material generates debris at a high temperature, which sticks to the contact surface between

the workpiece and the grinding disc, producing a large impact force on the grinding disc and decreasing the smooth operation of the entire device and a large vibration. Compared with the AlSiTiN–AlCrN coating, the AlSiTiN coating contains more Al, which strengthens the adhesion of the heat-resistant coating material of the cemented carbide workpiece and forms a dense, hard protective film. The Al_2O_3 film plays a protective and lubricating role on the coating surface, and the interior of the isolation coating is not oxidized, which enhances the oxidation resistance of the AlSiTiN coating. The integrity of the workpiece coating can effectively reduce friction between the grinding disc and the workpiece and reduce the vibration during the friction and wear process.

3.3. Influence of the Cr Coating on the Surface Friction and Wear Behavior

The friction force resulting from the friction and wear tests is shown in Figure 11. The friction force of the 27 groups of AlSiTiN coatings is generally greater than that of the AlSiTiN–AlCrN coatings, and the average value of the friction force data of the two coatings is also lower than that of the Cr-containing coating. This shows that the surface of the composite coating exhibits better wear resistance after adding an appropriate amount of Cr.
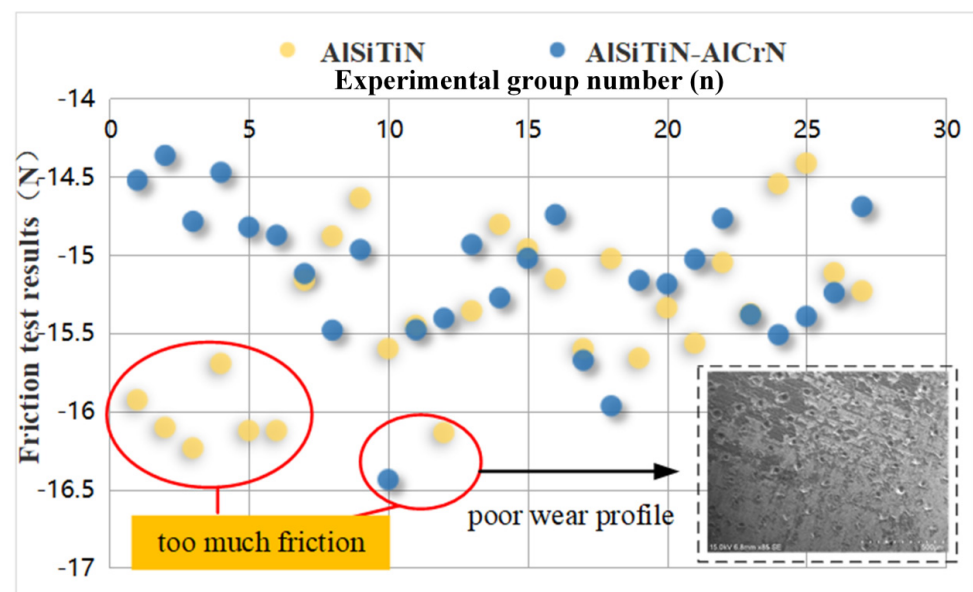

Figure 11. The results of the friction and wear test. (The illustration in the figure shows poor wear topography).

In the friction and wear process, the two friction surfaces contact each other under the action of pressure, and adhesion occurs in the process of relative sliding. In the AlSiTiN coating, Al and Ti play a major role in the friction and wear properties of the coating surface. Among them, the self-chip removal performance of Ti is poor, and the existence of wear debris at the friction interface accelerates the wear of the coating. Amorphous oxide TiO_2 with relatively weak wear resistance and poor chip removal performance is mainly formed during friction [17]. For the AlSiTiN–AlCrN coating, the addition of Cr induces a gradual appearance of the hard-phase nano-grains, such as metallic Cr and Cr-C compounds. The content of the Cr-C compound decisively determines the hardness of the composite coating, and the toughness of the coating is improved to a certain extent. In addition to surface scratching wear, there is oxidation wear in friction and wear experiments. The Cr in the coating can form stable, very hard, and heat-resistant oxides during the friction process. Thus, the AlSiTiN–AlCrN coating containing Cr exhibits a good chip removal performance during friction, and the friction coefficient is smaller than that of the AlSiTiN coating. The content of Ti is reduced due to the existence of Cr and Al in the

coating. As a result of their combined action, the addition of Al induces the formation of AlN, which improves the coating hardness and increases the resistance of the coating. In terms of grinding characteristics, the addition of Cr induced the formation of Cr_2O_3 in friction, which can improve the self-chip removal ability of the coating and has certain self-lubricating properties in friction and wear experiments, decreasing the friction coefficient. The microstructure, hardness, fracture toughness, and friction coefficient of the AlSiTiN–AlCrN coating directly affect the wear resistance of the coating. The lower the specific wear rate of the coating, the better the wear resistance.

Wear can be divided into adhesive wear, abrasive wear and fatigue wear according to friction surface damage. These wear forms often simultaneously appear in the wear process. Figure 12 shows the SEM images and elemental content of the specimen's surface in the friction and wear experiment. Figure 12a,b illustrate the surface topography of the AlSiTiN coating and the AlSiTiN–AlCrN coating, respectively. Figure 12c is the mean value of the elemental composition of the AlSiTiN coating scanned on the surface area of the AlSiTiN–AlCrN coating. Figure 12d is the local topography of adhesion wear, and Figure 12f is a partial magnified view of the surface morphology of oxidative wear.

Figure 12a,b shows that the surface wear morphology of the AlSiTiN–AlCrN coating is mostly better than that of the AlSiTiN coating. Moreover, the wear scar of the AlSiTiN coating is rough, the wear depth is large, and there is a lot of acceptable wear debris in the wear scar area. Compared with the AlSiTiN–AlCrN coating, the wear scar is shallower, and there is less wear debris. Figure 12c indicates that after adding Cr to the coating, the content of other elements does not change significantly, i.e., the fraction of Ti is the highest, followed by W. The content of Al is significantly reduced, from 13.05 to 5.56%, because Cr affects the phase composition of the coating, replacing the original AlN with Cr-nitride. Cr exists in the structure as Cr_2N and CrN. When the coating phase structure consists of the Cr_2N phase, the coating exhibits a high friction value. This is because the H_3/E_2 ratio of the Cr_2N phase is lower than that of the CrN phase, and Cr_2N easily reacts with oxygen in sliding contact to form Cr_2O_3 wear debris, which causes abrasive wear, resulting in a higher friction factor than CrN. The Cr nitrides have higher hardness and friction properties than AlN, and the atomic radius of Cr is smaller than that of Al; therefore, the Cr atoms in the AlSiTiN–AlCrN coating can be dissolved in the AlN lattice to cause lattice distortion, resulting in an obvious solid solution strengthening effect and improving the wear resistance of the coating. The friction properties of Cr_2N and CrN are better than those of AlN, so the wear resistance of AlSiTiN–AlCrN coating is better. This is consistent with the conclusion in the literature [18] that the corrosion resistance of experimental steels with different Cr element contents is equivalent, and the corrosion resistance is significantly better than that of ordinary carbon steel Q235 B. With the increase of time, the effect is more obvious. In addition, due to the addition of Cr, the α-Cr phase particles are produced in the surface structure of the specimen, which can improve the hardness of the metallographic structure. Furthermore, Cr is a strong carbide-forming element, which easily reacts with structural C to form high hardness carbides, so the hardness of the coating is significantly improved under the synergistic effect of the α-Cr phase and Cr carbides. The AlSiTiN–AlCrN coating exhibits a higher hardness, indirectly improving its surface wear resistance, thereby making a better surface morphology. In addition to the influence of Cr on the friction properties of the coating, other metal elements also play a certain role. Both coatings contain Si, which combines with O to form a SiO_2 or $Si(OH)_2$ layer, playing the role of self-lubrication and protection and reducing the friction coefficient of the coating.
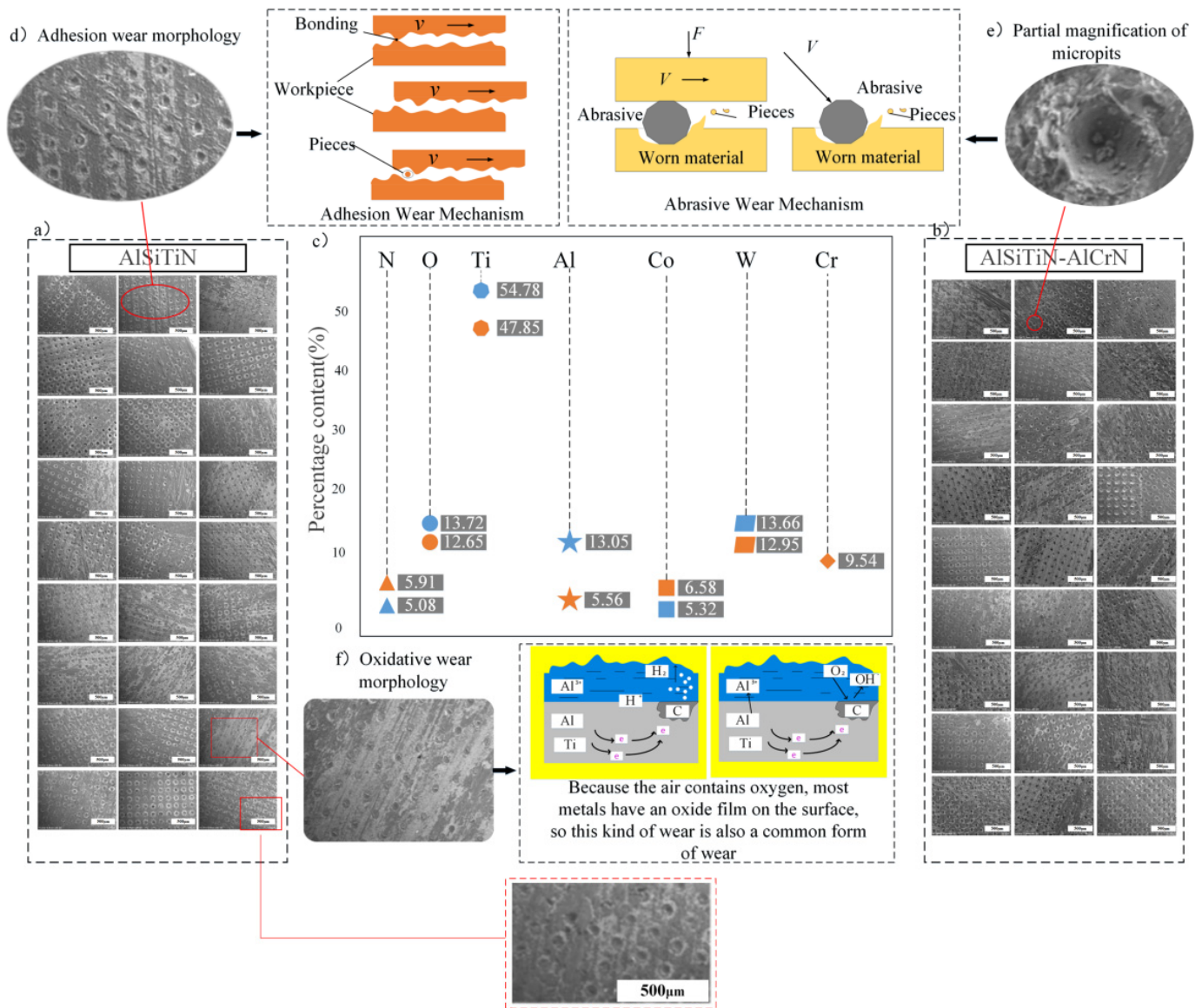
Figure 12. Wear morphology and the elemental content. (**a**) Wear morphology of AlSiTiN coating. (**b**) Wear morphology of AlSiTiN-AlCrN coating. (The scale of the images in (**a**,**b**) is 500 μm). (**c**) The mean value of the elemental composition of the AlSiTiN coating scanned on the surface area of the AlSiTiN–AlCrN coating. (**d**) Adhesion wear morphology. (**e**) Micro-pit local amplification map. (**f**) Friction principle diagram.

Figure 12c,d indicates that the content of O in the wear scar area of the two coatings is above 10%. This suggests that the wear mechanism may include oxidative wear because, under dry friction conditions, the temperature of the friction site continues to rise, resulting in chemical bonding between the coating and grinding ball atoms and oxygen from the air. The wear scar of the AlSiTiN coating is rough, and there is a lot of acceptable wear debris in the wear scar area. The main components in the wear scar area are Ti, W, O and Al, where the O content is 12.65%. However, the wear scar of the AlSiTiN–AlCrN coating is shallow, and a small part of wear debris exists in the wear scar area. The main components in the wear scar area are Ti, W, O and Cr, with an O content of 13.72%. Considering that Ti also causes adhesion wear, it is speculated that the wear mechanisms of both the AlSiTiN and AlSiTiN–AlCrN coatings are abrasive wear, adhesion wear, and oxidation wear.

4. Conclusions

(1)   Cr improves the hardness of the AlSiTiN–AlCrN coating because its addition leads to the generation of the α-Cr phase particles in the surface structure of the specimen. This results in good tissue stability. Cr is a strong carbide-forming element, and it reacts easier than W, Al and Ti with structural C to form very hard carbides. The synergistic effect of the two enhances the hardness of the AlSiTiN–AlCrN coating compared to the AlSiTiN coating. Moreover, the hardness value is relatively high when the content of Cr element is 29.8%–30.9%;

(2)   Cr affects the phase composition of the coating surface structure. The surface of the AlSiTiN–AlCrN coating with Cr and the AlSiTiN coating without Cr is very different. The atomic radius of Cr is smaller than that of Al, so the Cr atoms dissolve in the AlN lattice to cause lattice distortion. Cr preferentially interacts with electrons of C and N, suppressing the reaction of Al and Ti with non-metallic elements and the formation of final compounds;

(3)   Cr improves the wear resistance of the coating so that the coating exhibits better wear morphology. The addition of Cr forms Cr_2O_3 in friction, improves the coating hardness and the ability to remove chips, yielding better friction performance. However, adding Cr causes more mechanical damage due to the increase in hardness vibration.

Author Contributions: Conceptualization, X.T. and Q.Q.; methodology, Q.Q.; software, X.T.; validation, X.T., Y.Z. and P.H.; formal analysis, Y.Z.; investigation, P.H.; resources, X.T.; writing—original draft preparation, Y.Z.; writing—review and editing, Y.Z.; funding acquisition, X.T. All authors have read and agreed to the published version of the manuscript.

Institutional Review Board Statement: Not applicable.

Informed Consent Statement: Not applicable.

Data Availability Statement: Data presented in this study is available at request from the corresponding author.

Conflicts of Interest: The authors declare no conflict of interest.

References

1.   Zhang, H.; Xiong, J.; Guo, Z.; Yang, T.; Yi, J.; Yang, S.; Liang, L. Effect of WC particle size on high temperature wear resistance of WC-Co cemented carbide. *Hot Work. Technol.* **2022**, *2*, 21–24. Available online: https://www.leimingfadiant.com/periodical/d9dda2478cefd69149e78b01bc89ded2.html (accessed on 21 March 2023). (In Chinese).

2.   Tong, X.; Yang, S.; He, C.; Zheng, M. Multi-objective optimization of cutting performance of variable density micro-textured ball-end milling cutters. *Chin. J. Mech. Eng.* **2019**, *55*, 221–232. [CrossRef]

3.   Wang, L.; Guo, S.; Wei, Y.; Yuan, G. Experimental study on the effect of surface microtexture on the surface tribological properties of 45# steel friction pair. *Surf. Technol.* **2018**, *47*, 149–154. (In Chinese) [CrossRef]

4.   Guimarães, B.; Fernandes, C.M.; Figueiredo, D.; Carvalho, O.; Silva, F.S.; Miranda, G. Effect of laser surface texturing on the wettability of WC-Co cutting tools. *Int. J. Adv. Manuf. Technol.* **2020**, *111*, 1–9. [CrossRef]

5.   Zhang, J.; Wu, C.; Shi, X.; Xue, Y.; Huang, Q.; Zhang, K. Tribological Properties and Frictional Noise Behavior of Inconel 625 with Micro-texture Filled by Sn-Ag-Cu. *J. Mater. Eng. Perform.* **2021**, *31*, 82–93. [CrossRef]

6.   Xu, Y.; Han, X.; Xu, J.; Shan, Y.; Chen, Y.; Huang, R. Effects of laser surface texture micro-pit morphology and area occupancy on tribological properties of nitrided cylinder liners. *China Surf. Eng.* **2021**, *34*, 149–157. Available online: https://kns.cnki.net/kcms2/article/abstract?v=3uoqIhG8C44YLTlOAiTRKibYlV5Vjs7iy_Rpms2pqwbFRRUtoUImHZMo7JwiGryZiAMEWr6ipQ86wdmdQpIuzlNUd_L9-6ek&uniplatform=NZKPT (accessed on 22 September 2022).

7.   Zhang, Y. Micro Texture to Guide Research on the Effects of Friction and Wear Properties. Master's Thesis, Shandong University, Jinan, China, 2021. Available online: https://d.wanfangdata.com.cn/thesis/Y3814290 (accessed on 25 August 2021).
8.   Deng, J.; Li, S.; Xing, Y. Research progress on friction and wear characteristics of coated tools. *Manuf. Technol. Mach. Tools* **2012**, *1*, 59–63. Available online: https://m.fx361.com/news/2012/1020/15903302.html (accessed on 2 January 2012). (In Chinese).
9.   Dong, Y.; Shu, L.; Lin, R. Microstructure and friction and wear properties of laser cladding Fe-Cr-Mo-Si alloy coatings. *Adv. Laser Optoelectron.* **2021**, *58*, 1914007. (In Chinese)
10.   Zhang, Y.; Sun, H.; Wang, H.; Wang, X.; An, X.; He, K. Effects of Cr element on the crystal structure, microstructure, and mechanical properties of FeCrAl alloys. *Mater. Sci. Eng. A* **2021**, *826*, 142003. [CrossRef]
11.   Amanov, A.; Berkebile Stephen, P. Improvement in tribological behavior of thermal spray Cr_2O_3 and Cr_3C_2-NiCr coatings by ultrasonic nanocrystal surface modification. *Mater. Lett.* **2022**, *314*, 131919. [CrossRef]
12.   Zhang, E.; Wang, Q.; Zhang, S. Study on High Speed Milling Performance of CoCrMo Alloy with PVD Coating Tool. *Surf. Technol.* **2017**, *46*, 262–266. (In Chinese) [CrossRef]
13.   Zhang, M.; Wang, B.; Xu, S.; Tong, X.; Zhu, Z.; Gou, C. The effect of Cr on the microstructure and mechanical properties of G520 stainless steel welds. *Trans. China Weld. Inst.* **2021**, *42*, 52–57. (In Chinese) [CrossRef]
14.   Spadotto, J.C.; Burke, M.G.; Solórzano, I.G. Discontinuous Precipitation of α-Cr Phase in Alloy 33 (Cr-Fe-Ni-N). *Microsc. Microanal.* **2019**, *25*, 2650–2651. [CrossRef]
15.   Guo, J.; Shen, Y. Several problems should be paid attention to in the calculation of grain size by Scherrer formula. *J. Inn. Mong. Norm. Univ. (Nat. Sci. Ed.)* **2009**, *38*, 357–358. Available online: https://kns.cnki.net/kcms2/article/abstract?v=3uoqIhG8C44YLTlOAiTRKgchrJ08w1e75TZJapvoLK01sJiXUWyLrZHIIMA_aSdkUuCPKs-A0iMdUCMPyqLuip16Lv5f1BZq&uniplatform=NZKPT (accessed on 15 May 2009).
16.   Wang, J. Effect of Cr Element on microstructure and properties of High Strength Cold Rolled Weathering Steel. *Sci. Technol. Innov.* **2022**, 20–23. Available online: http://qikan.cqvip.com/Qikan/Article/Detail?id=7107681347 (accessed on 24 August 2022).
17.   Liu, L.; Lv, Z.; Liu, B.; Xie, R. Effect of Ti on the Distribution and hardness of precipitated phase in ODS steel containing 9% Cr. *J. Heat Treat. Mater.* **2022**, *43*, 94–103. (In Chinese) [CrossRef]
18.   Hao, F.; Liu, K. Effect of Cr on Corrosion Resistance of HRB400E Steel Bar. *Manuf. Upgrad. Today* **2022**, 68–70. Available online: http://qikan.cqvip.com/Qikan/Article/Detail?id=7106778387&from=Qikan_Search_Index (accessed on 15 January 2022).